Supplementary Information

Structure of nanoscale-pitch helical phases: blue phase and twist-bend nematic phase resolved by resonant soft X-ray scattering

M. Salamończyk, N. Vaupotič, D. Pociecha, C. Wang, C. Zhu, E. Gorecka

1. *Supplemental discussion on theoretical modelling*

Modulated nematic phases:

Due to the uniform electron density, the elastic x-ray scattering in nematic phases detects only a short range positional order of molecules, while the resonant scattering [1, 2] provides the information on a non-uniform orientational structure of molecules. To calculate the dispersion correction to the form factor we start from the x-ray polarizability of a molecule written in the eigen system of the molecule with the long molecular axis along the z-axis. We assume [3], that the form factor in the eigen system (F_{ei}) has a form of a traceless tensor (as does the anisotropic part of the polarizability tensor):

$$F_{ei} = \begin{pmatrix} f_1 & 0 & 0 \\ 0 & f_2 & 0 \\ 0 & 0 & -(f_1+f_2) \end{pmatrix}.$$

In the N_{TB} phase the averaged direction of the long molecular axes (director) is inclined from the z axis of the laboratory frame and rotates along the laboratory z axis (Fig. S1(a)), while in the N_{SB} phase, the director oscillates along the z axis (Fig. S1(b)). The cholesteric phase can be described as a special case of the N_{TB} phase with a conical angle equal to 90 degrees.

The dispersion correction in the laboratory system is obtained by the rotation of the molecular coordinate system. In the N_{TB} phase we first rotate it by an angle θ_{TB} (the conical angle) around the y axis and then by an angle $\varphi = q_{TB}z$ around the z axis. The dispersion correction tensor for the N_{TB} phase is thus

$$F^{(TB)} = R_\varphi^T\left(R_\theta^T F_{ei} R_\theta\right)R_\varphi \ ,$$

where R_θ is:

$$R_\theta = \begin{pmatrix} \cos\theta_{TB} & 0 & \sin\theta_{TB} \\ 0 & 1 & 0 \\ -\sin\theta_{TB} & 0 & \cos\theta_{TB} \end{pmatrix}$$

and R_φ is

$$R_\varphi = \begin{pmatrix} \cos\varphi & \sin\varphi & 0 \\ -\sin\varphi & \cos\varphi & 0 \\ 0 & 0 & 1 \end{pmatrix} .$$

Calculating the Fourier transform of $F^{(TB)}$ ($F_q^{(TB)}$), we find that the elements of the dispersion correction tensor are different from zero only when q_z has one of the following values: 0, $\pm q_0$ or $\pm 2q_0$, where $q_0 = 2\pi/L$ is the magnitude of the wave vector of the heliconical deformation with the pitch L. If $q_z = q_0$, the dispersion correction to the form factor is:

$$F_{q_0}^{(TB)} = \left(f_1 + \frac{f_2}{2}\right)\sin(2\theta_{TB})\begin{pmatrix} 0 & 0 & 1 \\ 0 & 0 & i \\ 1 & i & 0 \end{pmatrix}$$

and if $q_z = 2q_0$:

$$F_{2q_0}^{(TB)} = \left[\frac{1}{2}(f_1 - f_2) + \left(f_1 + \frac{f_2}{2}\right)\sin^2\theta_{TB}\right]\begin{pmatrix} 1 & i & 0 \\ i & -1 & 0 \\ 0 & 0 & 0 \end{pmatrix} .$$

In order to find the dispersion correction tensor in the N_{SB} phase we repeat the above procedure, but in this case we have to rotate the director around the y axis by an angle $\theta = \theta_{SB}\sin q_0 z$, where θ_{SB} is the magnitude of the modulation angle and q_0 is the modulation wave vector. As the splay-bend modulation can be within any plane containing the z axis, the resulting structure is then rotated around the z axis by an angle φ to obtain the dispersion correction tensor for a domain with an arbitrarily oriented modulation plane. The elements of the tensor obtained in this way cannot be Fourier-transformed analytically, so we Taylor expand the tensor elements up to the second order in θ_{sb}. If $q_z = q_0$, the dispersion correction to the form factor is:

$$F_{q_0}^{(SB)} = 2i\left(f_1 + \frac{f_2}{2}\right)\theta_{sb}\begin{pmatrix} 0 & 0 & \cos\varphi \\ 0 & 0 & \sin\varphi \\ \cos\varphi & \sin\varphi & 0 \end{pmatrix}$$

and if $q_z = 2q_0$:

$$F_{2q_0}^{(SB)} = \left(f_1 + \frac{f_2}{2}\right)\theta_{sb}^2\begin{pmatrix} \cos^2\varphi & \cos\varphi\sin\varphi & 0 \\ \cos\varphi\sin\varphi & \sin^2\varphi & 0 \\ 0 & 0 & -1 \end{pmatrix} .$$

Next we study the effect of the polarization of the incident beam on the scattered light. Let the incident beam propagate along the y axis of laboratory frame (Fig. S2) and is polarized along the x axis. The constructive x-ray interference will be observed from those parts of the sample, in which the modulation axis is tilted by an angle $\pi/2 - \theta_{sc}/2$ with respect to the direction of the incident beam, where θ_{sc} is the scattering angle, i.e. for all the modulation axes lying on the cone, as shown in Fig. S2. For the modulation axis in the yz plane, the incident beam is σ-polarized. For

the modulation axis in the xy plane this incident beam is π-polarized and for the other directions on the cone the incident beam has both the σ and π component.

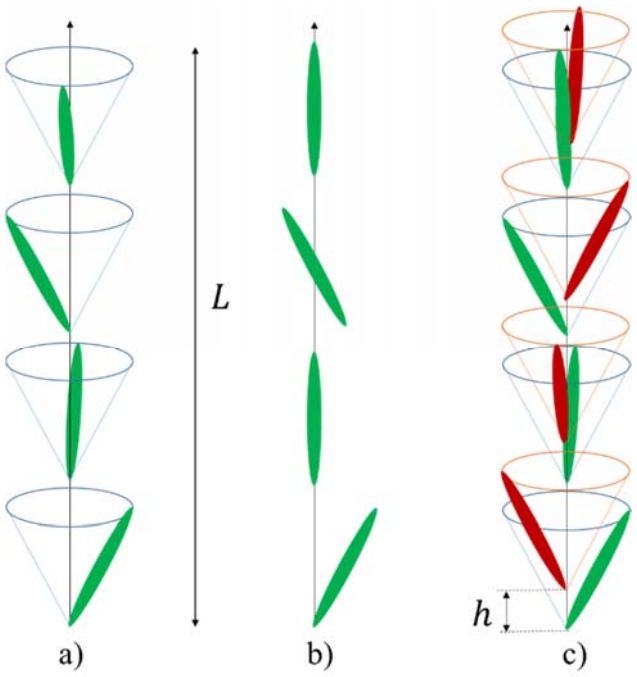

Fig. S1. Schematic presentation of the a) N_{TB} and b) N_{SB} phase. c) Modulated nematic phase with two helices with molecules on the opposite side of the cone, shifted by h.

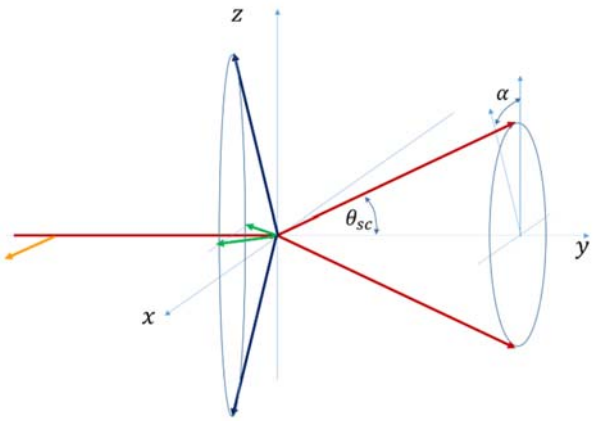

Fig. S2. Scattering geometry (in the laboratory frame). The incident beam propagates along the y axis and is polarized along the x axis (orange arrow). The scattering is constructive for all the directions of the heliconical axes lying on the cone. For the directions of the helix axes denoted by blue arrows the incident beam is σ-polarized and for the "green" directions the beam is π-polarized. The scattering angle is θ_{sc} and α is the azimuthal angle.

Supplementary Information

For the beam scattered at the azimuthal angle α the σ and π components of the incident beam are:

$$\vec{\sigma}_{in} = (\cos\alpha\,, 0,0)\ ,\ \vec{\pi}_{in} = (0,0,\sin\alpha\,)$$

and for the scattered beam the directions of the σ and π component are:

$$\vec{\sigma}_{sc} = (1,0,0)\,, \vec{\pi}_{sc} = (0, -\sin\theta_{sc}\,, \cos\theta_{sc}\,)\quad .$$

The amplitudes of the σ and π components of the scattered light are found as [2]:

$$A_{\sigma\sigma} = \sum_{i,j} \sigma_{sc,j} F'_{ij} \sigma_{in,i}\quad ,$$
$$A_{\sigma\pi} = \sum_{i,j} \pi_{sc,j} F'_{ij} \sigma_{in,i}\quad ,$$
$$A_{\pi\sigma} = \sum_{i,j} \sigma_{sc,j} F'_{ij} \pi_{in,i}\quad ,$$
$$A_{\pi\pi} = \sum_{i,j} \pi_{sc,j} F'_{ij} \pi_{in,i}\quad .$$

where the elements of the tensors F'_{ij} are the elements of tensors $F_{q_0}^{(TB)}$, $F_{2q_0}^{(TB)}$, $F_{q_0}^{(SB)}$ or $F_{2q_0}^{(SB)}$ rotated by an angle $\theta_{sc}/2$ around the x axis:

$$F'_{ij} = R^{T}_{\theta_{sc}/2} F^{(TB,SB)}_{q_0,2q_0} R_{\theta_{sc}/2}\quad ,$$

with

$$R_{\theta_{sc}/2} = \begin{pmatrix} 1 & 0 & 0 \\ 0 & \cos\left(\frac{\theta_{sc}}{2}\right) & \sin\left(\frac{\theta_{sc}}{2}\right) \\ 0 & -\sin\left(\frac{\theta_{sc}}{2}\right) & \cos\left(\frac{\theta_{sc}}{2}\right) \end{pmatrix}$$

for the helix axis to be in the proper direction with respect to the incident beam for the constructive interference to occur. It is enough to rotate the tensor only about the x-axis (and not also around the y-axis), because all the directions of the helix axis on the cone that lead to constructive interference at some angle α on the screen (see Fig. S2) are taken into account by considering all the possible directions of the polarization of the incoming beam.

The intensity of the scattered light is then calculated as [2]

$$I = |A_{\sigma\sigma}|^2 + |A_{\pi\sigma}|^2 + |A_{\sigma\pi}|^2 + |A_{\pi\pi}|^2 \quad .$$

Keeping only the relevant factors required to compare the relative magnitudes of intensities, we find for the N_{TB} phase:

$$I_{q_0}^{(TB)} = \sin^2(2\theta_{TB}) \cos^2\left(\frac{\theta_{sc}^{(q_0)}}{2}\right),$$

$$I_{2q_0}^{(TB)} = \frac{\left(-\frac{3}{f_{12}} + (2f_{12}+1)\cos(2\theta_{TB})\right)^2}{4(2f_{12}+1)^2}\left(1 + \sin^2\left(\frac{\theta_{sc}^{(2q_0)}}{2}\right)\right) \times \left(\cos^2\alpha + \sin^2\left(\frac{\theta_{sc}^{(2q_0)}}{2}\right)\sin^2\alpha\right)$$

and for the N_{SB} phase:

$$I_{q_0}^{(SB)} = 2\,\theta_{sb}^2 \cos^2\left(\frac{\theta_{sc}^{(q_0)}}{2}\right),$$

$$I_{2q_0}^{(SB)} = \frac{1}{64}\theta_{sb}^4 \left[4\cos^2\alpha\left(7 - \cos\theta_{sc}^{(2q_0)}\right) + \left(45 + 16\cos\theta_{sc}^{(2q_0)} + 3\cos\left(2\theta_{sc}^{(2q_0)}\right)\right)\sin^2\alpha\right] .$$

In the calculation of the scattering intensity in the N_{SB} phase we have averaged over all the possible orientations of the splay-bend plane. The value of the parameter $f_{12} = f_1/f_2$ determines the intensity of the $2q_0$ peak with respect to the intensity of the q_0 peak in the N_{TB} phase. If $f_{12} \geq 1$ the intensity of the $2q_0$ peak is approximately two orders of magnitude lower than the intensity of the q_0 peak. If $f_{12} < 1$, the intensity of the $2q_0$ peak increases rapidly. The intensity scattered from a powder sample as a function of the azimuthal angle on the screen for the incident beam along the y direction and polarized along the x axis, is given in Fig. S3.

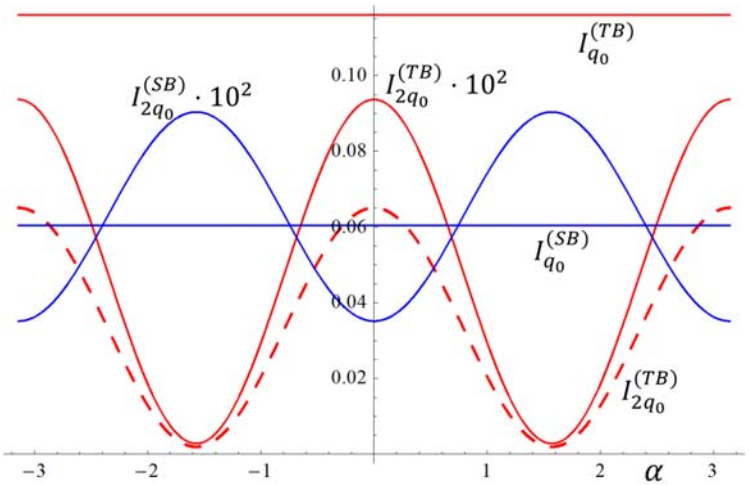

Fig. S3. The intensity (I) of the scattered beam (in arbitrary units) as a function of the azimuthal angle α. The scattering geometry is shown in Fig. S2; blue lines: N_{SB}; red lines: N_{TB}; the red solid line for the $2q_0$ intensity: $f_{12} = 0.8$ and red dashed line: $f_{12} = 1.0$. Parameter values: $\theta_{sc}(q_0) = 10°$, $\theta_{TB} = 10°$.

Experimentally, only one diffraction peak is observed in the modulated nematic phase with no clear dependence of the intensity on the direction of the polarisation of the incident beam. We can therefore conclude that the observed signal corresponds to the full pitch band (q_0) in either the N_{TB} or N_{SB} modulated nematic phase. The N_{SB} phase should be optically biaxial. Experimentally, no biaxiality is observed, so in the further discussion we focus on the N_{TB} phase. The half pitch band (the $2q_0$ peak) should be strongly polarization dependent. Assuming $f_{12} \approx 1$, the intensity of this signal is expected to be much lower than for the full pitch band (Fig. S4). However, as we will show later in the study of the blue phases, we can expect that the parameter f_{12} is lower than 1 and in that case the $2q_0$ signal intensity in the N_{TB} phase becomes comparable to the intensity of the q_0 peak (Fig. S4(b)).

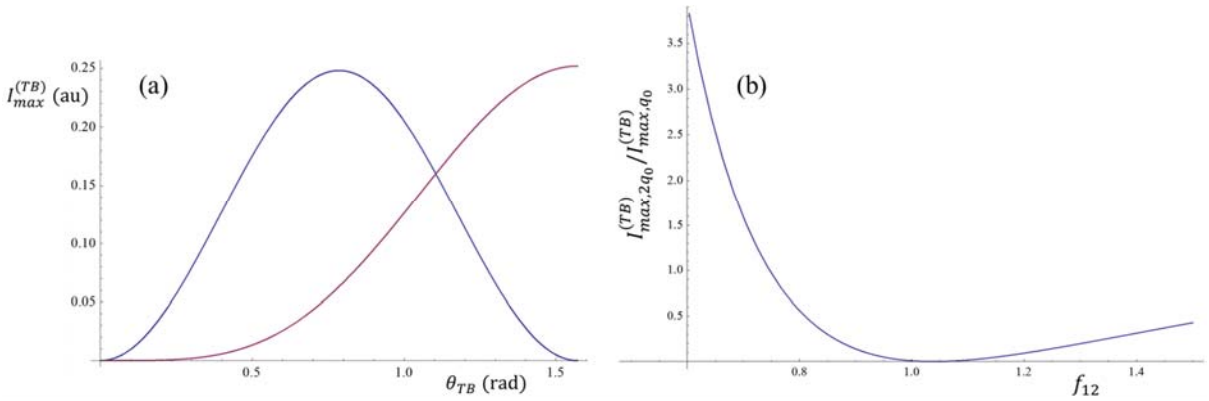

Fig. S4. (a) The maximum intensity (I_{max}) of the q_0 peak (blue) and the maximum intensity of the $2q_0$ peak (violet) in the N_{TB} phase as a function of the heliconical angle θ_{TB}. Parameter values: $f_{12} = 1$, $\theta_{sc}(q_0) = 10°$. (b) The ratio between the maximum intensity of the $2q_0$ and q_0 peaks in the N_{TB} phase as a function of the parameter f_{12} at $\theta_{TB} = 10°$, $\theta_{sc}(q_0) = 10°$ and $\theta_{sc}(2q_0) = 20°$.

Possible reasons for the suppression of the $2q_0$ peak are discussed in the main text. Because the $2q_0$ peak has not been observed in any of the NTB material studied so far, this can be a hint to search for a more fundamental reason, i. e. the structure of N_{TB} might not be of a simple heliconical type. Therefore, we considered a modification of the N_{TB} structure, assuming that it is built of two interlocked helical modulations mutually shifted as shown in Fig. S1(c). The dispersion corrections to the form factor for such a structure are easy to obtain. We add the form factors for two interlocked helices, including the phase shift between them, noting that $F_{2q0}^{(TB)}$ is an even and $F_{q0}^{(TB)}$ is an odd function in θ_{TB}, and obtain:

$$F_{2q_0} = F_{2q_0}^{(TB)}\left(1 + e^{i2q_0h}\right) ,$$
$$F_{q_0} = F_{q0}^{(TB)}\left(1 - e^{iq_0h}\right) .$$

If $q_0 h \ll 1$, the dispersion correction to the form factor goes to zero for the q_0 peak, as expected from the symmetry consideration only (the pitch length reduces to $L/2$). If, however, the second helix is shifted by $L/4$, then the intensity of the $2q_0$ peak is zero. It should be pointed out, that the intensity of the $2q_0$ peak is zero if the helix is shifted by $L/4$ and the molecules are on the opposite side of the cone, as shown in Fig. S1, but it is zero also for a pure shift by $L/4$ (with the molecules staying at the same side of the cone).

Blue phase II:

The position of the non-resonant peaks in the blue phase II (BPII) is calculated in the following way. An infinite line of a uniform electron density along the cylinder axis (Fig. S5(a)) represents a cylinder. The lines of uniform density, as shown in Fig. S5(b), represent the defects. The scattering vector $\vec{q}$ is given by $\vec{q} = q_l(h,k,l)$, where $q_l = \frac{2\pi}{a}$ and a is the size of the crystallographic unit cell (and equals half the pitch of the helix, see Fig. S5(a)) and h, k and l are the Miller indices.

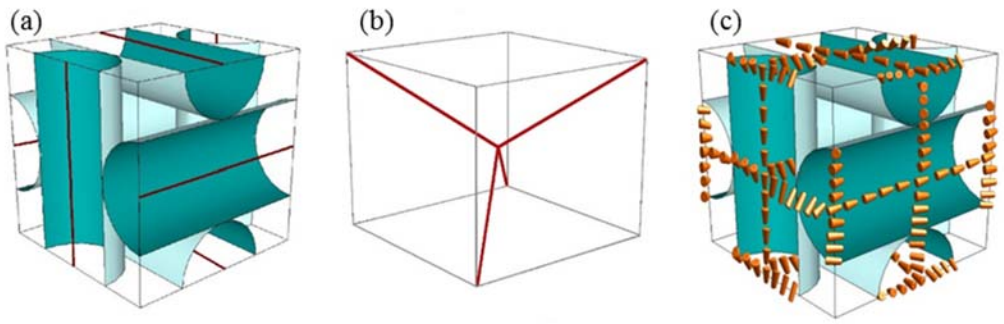

Fig. S5. Structure of the BPII phase. In the calculation of the form factor of the unit cell the cylinders (a) and defects (b) are represented by lines. (c) In the calculation of the tensorial correction to the form factor we consider spatial variation of the director in the direction perpendicular to the cylinder long axis.

The BPII phase consists of cylinders with their axes along the x, y and z direction. The Fourier transform of each line representing a cylinder gives a delta function, either $\delta(q_x)$, $\delta(q_y)$ or $\delta(q_z)$, where q_i, $i = x, y, z$, are the components of the scattering vector. Taking into account the position of the cylinders in the unit cell we find the following form factor (F_c) for the BPII phase:

$$F_c = \delta(q_x) + \delta(q_y)e^{i\pi(h+l)} + \delta(q_z)e^{i\pi k} \ .$$

From the expression for F_c it follows, that at least one of the indices h, k or l has to be zero in order to have the form factor different from zero. If only one index is zero, the form factor is always different from zero. If two indices are zero, then the nonzero index has to be an even number to obtain a nonzero form factor; thus there is no $(0,0,1)$ peak, but there is a $(0,0,2)$ peak.

Supplementary Information

The defect lines run along $\frac{a}{2}(1,1,1)+\lambda(-1,1,1)$, $\frac{a}{2}(1,1,1)+\lambda(1,-1,1)$, $\frac{a}{2}(1,1,1)+\lambda(1,1,-1)$ and $\frac{a}{2}(1,1,1)-\lambda(1,1,1)$, where $\lambda \in \left[0,\frac{a}{2}\right]$. We assume, that along the defect lines the electron density differs from the electron density of the surrounding, so the form factor related to the defects (F_d) is given by the Fourier transform of the electron density along the defect lines. We find:

$$F_d = \frac{(1-e^{-i(h+k-l)\pi})}{h+k-l}e^{2i(h+k)\pi} + \frac{(1-e^{-i(h-k+l)\pi})}{h-k+l}e^{2i(h+l)\pi} + \frac{(1-e^{-i(-h+k+l)\pi})}{-h+k+l}e^{2i(k+l)\pi} - \frac{1-e^{i(h+k+l)\pi}}{h+k+l} \quad .$$

The non-zero intensity peaks are given in Table S1. Note, that the defects do not give any $(0,0,l)$ peaks.

Table S1. Theoretically calculated peaks. Ticks denote the peaks for which a non-zero intensity is predicted. In the BPI, the (002) peak is a purely resonant peak and in BPII, the (001) peak is a resonant peak. The yellow and light green areas denote the peaks allowed by the $I4_132$ symmetry of the BPI phase and the $P4_232$ symmetry of the BPII phase, respectively. Note, that the (031) peak in the BPI is not resonantly enhanced. The peak (222) is not marked as purely resonant because it is allowed by the $I4_132$ symmetry; it is a coincidence that for the chosen model of the electron density (along the cylinder axis and the defect lines) the intensity in the elastic scattering is zero. The magnitude of the lattice wave vector is q_l and the magnitude of the wave vector corresponding to the director modulation is q_0.

	BP-II ($q_l = 2q_0$)			**BP-I ($q_l = q_0$)**		
Peak (hkl)	Elastic due to cylinders	Elastic due to defects	Resonant/resonantly enhanced	Elastic due to cylinders	Elastic due to defects	Resonant/resonantly enhanced
(001)	×	×	✓	×	×	×
(011)	✓	✓	✓	✓	×	✓
(111)	×	✓	✓	×	×	×
(002)	✓	×	✓	×	×	✓
(021)	✓	×	✓	×	×	×
(211)	×	✓	✓	×	✓	✓
(022)	✓	✓	✓	✓	✓	✓
(221)	×	✓	✓	×	×	×
(031)	✓	×	✓	✓	×	×
(311)	×	✓	✓	×	×	×
(222)	×	×	×	×	×	✓
(032)	✓	×	✓	×	×	×
(321)	×	✓	✓	×	✓	✓

Supplementary Information

It is important to point out, that in the elastic x-ray scattering, although allowed by the symmetry, none of the diffraction signals will be observed, because the cylinders are in close contact (i.e. the density in the unit cell is almost uniform) and the density difference between the defect lines and cylinders, if any, is very low, because the phase has only a short range positional order. However, as shown below, the peaks observed in the resonant x-ray scattering are actually at the positions expected for the non-resonant peaks due to the 'resonant enhancement' effect [5, 6].

As in the case of the modulated nematic phase, to calculate the dispersion correction to the form factor, we consider the molecules having a rod-like shape. We present the calculations starting from the anisotropic traceless tensor F_{ei} in the eigensystem, this time assuming that $f_1 = f_2$ in order to make the analytical results not too complicated. At the end we shall comment on the effect of $f_1 \neq f_2$.

With the x-axis along the average orientation of the long molecular axis, the anisotropic traceless tensor is:

$$F_{ei} = \begin{pmatrix} -2f_1 & 0 & 0 \\ 0 & f_1 & 0 \\ 0 & 0 & f_1 \end{pmatrix} .$$

Because the long molecular axis rotates, for example, along the z axis (see Fig. S5(c)), the tensorial dispersion correction in the laboratory frame is obtained as

$$F = R^T F_{ei} R \quad ,$$

where R is a rotation matrix:

$$R = \begin{pmatrix} \cos(q_0 z) & \sin(q_0 z) & 0 \\ -\sin(q_0 z) & \cos(q_0 z) & 0 \\ 0 & 0 & 1 \end{pmatrix} .$$

q_0 is the wave vector of the nematic director modulation and its magnitude is half the magnitude of the lattice wave vector q_l. We find (omitting all the irrelevant factors) that the dispersion correction to the form factor due to the helical rotation of the long molecular axis along the z direction (F_z) is:

$$F_z = f_1 \begin{pmatrix} -\delta(q_z) - \frac{3}{2}\,\delta(q_z \pm q_l) & \pm\frac{3}{2} i\,\delta(q_z \pm q_l) & 0 \\ \pm\frac{3}{2} i\,\delta(q_z \pm q_l) & -\delta(q_z) + \frac{3}{2}\,\delta(q_z \pm q_l) & 0 \\ 0 & 0 & 2\delta(q_z) \end{pmatrix} .$$

The dispersion correction depends only on the z component of the scattering vector and it is different from zero only for $l = 0$ or $l = 1$. Similarly, we find the dispersion correction due to the rotation along the x (F_x) and y direction (F_y). The dispersion correction to the form factor (F_{hkl}) of the unit cell is:

$$F_{hkl} = F_x\,(h)e^{i\pi k} + F_y(k)e^{i\pi l} + F_z(l)e^{i\pi h} \quad .$$

The full expression of F_q is too comprehensive to be written in full, so we give some specific examples. First, we point out, that the resonant scattering should give one peak, which is forbidden in the elastic scattering, the $(0,0,1)$ peak. We also point out that those peaks, which have at least one of the Miller indices either 0 or 1, are resonantly enhanced, because this is the required condition for at least one dispersion correction to the form factor (F_x, F_y or F_z) to be different from zero.

Blue phase I:

We shall now repeat the above-described procedure to calculate the elastic and resonant peaks of the BPI phase. The schematic presentation of the BPI is shown in Fig. S6. To calculate the peaks allowed by the elastic x-ray scattering we again represent the structure of the double twist cylinders and defects as lines of a non-zero electron density and find:

$$F_c = \frac{1}{h}\left(-1+e^{2ih\pi}\right)\left(e^{\frac{ik\pi}{2}} + e^{\frac{1}{2}i(3k+2l)\pi}\right) + \frac{1}{k}\left(-1+e^{2ik\pi}\right)\left(e^{\frac{3il\pi}{2}} + e^{\frac{1}{2}i(2h+l)\pi}\right) + \frac{1}{l}\left(-1+e^{2il\pi}\right)\left(e^{\frac{ih\pi}{2}} + e^{\frac{1}{2}i(3h+2k)\pi}\right)$$

and

$$F_d = -\frac{i\left(e^{ih\pi} - e^{i(-h+2(k+l))\pi}\right)}{2(h-k-l)\pi} - \frac{i\left(e^{2i(h+k)\pi} - e^{2il\pi}\right)}{2(h+k-l)\pi} + \frac{i\left(e^{i(2k+l)\pi} - e^{i(2h+3l)\pi}\right)}{2(h-k+l)\pi} + \frac{i\left(e^{ik\pi} - e^{i(k+2(h+k+l))\pi}\right)}{2(h+k+l)\pi} \quad .$$

The peaks allowed by the symmetry of the BPI phase are given in Table S1.

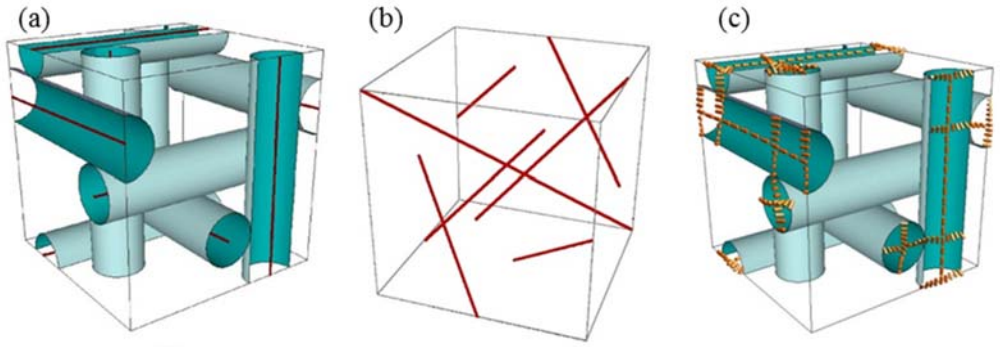

Fig. S6. Structure of the BPI phase. In the calculation of the form factor of the unit cell the (a) cylinders and (b) defects are represented by lines. (c) In the calculation of the tensorial correction to the form factor we consider spatial variation of the director in the direction perpendicular to the cylinder long axis.

Supplementary Information

To calculate the allowed resonant peaks we repeat the procedure used for the BPII phase, taking into account the positions of the helical double twist cylinders in the BPI phase. An excellent presentation of the structure in the BPI phase is available in the video clip [7]. There, it can be seen, that at each crossing of two cylinders there is a helical deformation of the orientation of long molecular axes. The long molecular axis rotates by π when moving from the surface of one cylinder to the surface of the other one (see Fig.S 6(c)). So, the major difference with the BPII phase is, that now we do not have infinite helices, but several half-pitch helices in each unit cell.

To calculate the dispersion correction to the form factor of the unit cell there are a few more points to be considered. In calculating the traceless anisotropy tensor in the laboratory system for the helices along the x, y and z axis, we follow the procedure given for the BPII phase. If the long molecular axis rotates around the z-direction, the rotation angle (φ_z) is expressed as $\varphi_z = \pm\frac{\pi}{4} - q_0 z$ and in the integration (when calculating the Fourier transform) z runs from 0 to π/q_0 (note, that in the BPI phase $q_0 = q_l$). By choosing the orientation of the molecules in one cylinder, we have defined the orientation of molecules in all cylinders. In addition, we choose, that the rotations along the z axis are clockwise, and that the orientation of the long molecular axis is along the x axis if $\varphi_z = 0$.

Similarly, for the helices along the x axis, we set $\varphi_x = 0$ for the long molecular axis along the y axis and then find that the rotation is clock-wise, thus $\varphi_x = \pm\frac{\pi}{4} - q_0 x$. For the helices along the y axis, the long molecular axis is along the z axis at $\varphi_y = 0$, the rotation is anticlock-wise and $\varphi_y = \pm\frac{\pi}{4} + q_0 y$.

There are 12 helices in one unit cell. For each one of them the initial φ, which is either $\pi/4$ or $-\pi/4$, has to be determined and then the phase factor due to the position of the helix has to be added to the proper form factor. Finally, we obtain the dispersion correction (F_{hkl}) to the form factor:

$$\begin{aligned} F_{hkl} = F_x^{(-)}\left(e^{2i\pi(h/8+0/8k+2/8l)} + e^{2i\pi(5h/8+4/8k+6/8l)}\right) \\ + F_x^{(+)}\left(e^{2i\pi(-h/8+0/8k+6/8l)} + e^{2i\pi(3h/8+4/8k+2/8l)}\right) \\ + F_z^{(+)}\left(e^{2i\pi(4h/8+2/8k-1/8l)} + e^{2i\pi(0h/8+6/8k+3/8l)}\right) \\ + F_z^{(-)}\left(e^{2i\pi(4h/8+6/8k+1/8l)} + e^{2i\pi(0h/8+2/8k+5/8l)}\right) \\ + F_y^{(+)}\left(e^{2i\pi(6h/8+1/8k+0/8l)} + e^{2i\pi(2h/8+5/8k+4/8l)}\right) \\ + F_y^{(-)}\left(e^{2i\pi(6h/8+3/8k+4/8l)} + e^{2i\pi(2h/8-1/8k+0/8l)}\right) \ , \end{aligned}$$

where $F_{x,y,z}$ are the Fourier transforms of the helices along the x, y and z axis, respectively, and the index + or – denotes the helix, in which the initial φ is $\pi/4$ or $-\pi/4$, respectively. The expression for F_x is:

$$F_x^{(\pm)} = \begin{pmatrix} F_{11}^{(\pm)} & 0 & 0 \\ 0 & F_{22}^{(\pm)} & F_{23}^{(\pm)} \\ 0 & F_{23}^{(\pm)} & F_{33}^{(\pm)} \end{pmatrix}$$

with

$$F_{11}^{(\pm)} = f_1 \frac{i\left(1 - e^{ih\pi}\right)}{h} ,$$

$$F_{22}^{(\pm)} = if_1 \frac{\left(1 - e^{ih\pi}\right)(-4 \pm 6ih + h^2)}{2h(4 - h^2)} ,$$

$$F_{23}^{(\pm)} = F_{23}^{(\pm)} = \pm 3if_1 \frac{\left(1 - e^{ih\pi}\right)h}{2(4 - h^2)} ,$$

$$F_{33}^{(\pm)} = if_1 \frac{\left(1 - e^{ih\pi}\right)(-4 \mp 6ih + h^2)}{2h(4 - h^2)} .$$

Therefore, $F_x^{(\pm)}$ depends only on the Miller index h. The expressions for the other two tensors can be deduced from the above expressions: h has to be replaced by k or l and the zeros are in the second or third line of the tensor.

In the BPI phase, the purely resonant peak (the peak not allowed by the $I4_132$ symmetry) is the (002) peak. The rest of the signals are allowed by the $I4_132$ symmetry, but are observed only in the resonant x-ray scattering due to the resonant enhancement: (011), (211), (022), (222), (321). However, not all the signals allowed by the $I4_132$ symmetry that are observed in the resonant experiment are resonantly enhanced, e.g. the (031) signal. The presence of a very week (031) signal in the RSoXS pattern might indicate that there is some distortion of the helical structure of the double twist cylinders.

Next, we study the effect of the polarization of the incident beam on the intensity of the scattered beam. As before, we choose the direction of the incident beam to be along the y axis and is polarized along the x axis. For the scattered light with the $\vec{q}$-vector lying in the yz plane, the incident beam is σ-polarized, for $\vec{q}$ in the xy plane it is π-polarized and for all the other direction both σ and π components are present. To obtain the amplitudes of the scattered light the procedure is more comprehensive than in the case of the modulated nematic phase. To show it, we consider the (002) peak as an example. The multiplicity of this peak is 6: (00 ± 2), (0 ± 20) and (± 200). First, we calculate the dispersion correction of a given peak and for the positive values of the Miller index 2 we find:

$$F_{002} = f_1 \begin{pmatrix} -3 & i & 0 \\ i & 3 & 0 \\ 0 & 0 & 0 \end{pmatrix}, \; F_{020} = f_1 \begin{pmatrix} 3 & 0 & i \\ 0 & 0 & 0 \\ i & 0 & -3 \end{pmatrix}, \; F_{200} = f_1 \begin{pmatrix} 0 & 0 & 0 \\ 0 & -3 & i \\ 0 & i & 3 \end{pmatrix}.$$

To have the $\vec{q}$ vector along the x, y or z axis, one should choose a proper direction of the incident beam. Since we have fixed the direction of the incident beam, we have to find those crystals in the powder sample, that will have their local x, y or z axis (for which the above expressions of F_{hkl}

apply) at a proper angle with respect to the direction of the incoming beam. The directions of these $\vec{q}(hkl)$ in the laboratory system are defined by angles θ_0 and φ_0, defining the angle between the laboratory z axis and $\vec{q}(hkl)$ and the y axis and $\vec{q}(hkl)$, respectively. For $\vec{q}(002)$ both angles are zero, for $\vec{q}(020)$ $\varphi_0 = 0$ and $\theta_0 = \pi/2$ and for $\vec{q}(200)$ $\varphi_0 = \pi/2$ and $\theta_0 = \pi/2$. We thus have to rotate the F_{hkl} tensor by

$$F'_{hkl} = R^T_{\theta_0}\left(R^T_{\varphi_0} F_{hkl} R_{\varphi_0}\right) R_{\theta_0} \ ,$$

where

$$R_{\varphi_0} = \begin{pmatrix} \cos\varphi_0 & \sin\varphi_0 & 0 \\ -\sin\varphi_0 & \cos\varphi_0 & 0 \\ 0 & 0 & 1 \end{pmatrix}$$

and

$$R_{\theta_0} = \begin{pmatrix} 1 & 0 & 0 \\ 0 & \cos\left(\frac{\theta_{sc}}{2} + \theta_0\right) & \sin\left(\frac{\theta_{sc}}{2} + \theta_0\right) \\ 0 & -\sin\left(\frac{\theta_{sc}}{2} + \theta_0\right) & \cos\left(\frac{\theta_{sc}}{2} + \theta_0\right) \end{pmatrix} \ .$$

As in the case of modulated nematics, for the beam scattered at the azimuthal angle α (see Fig. S2), the σ and π components of the incident beam are:

$$\vec{\sigma}_{in} = (\cos\alpha\,, 0, 0) \ ,$$
$$\vec{\pi}_{in} = (0, 0, \sin\alpha\,) \ .$$

For the scattered beam the directions of the σ and π component are:

$$\vec{\sigma}_{sc} = (1,0,0) \ ,$$
$$\vec{\pi}_{sc} = (0, -\sin\theta_{sc}\,, \cos\theta_{sc}\,) \ ,$$

where the magnitude of the scattering angle depends on the chosen peak. The intensity of the scattered peak is now calculated following the procedure given in previous section. In the case of the (002) peak there are 6 contributions to the intensity of this peak and they are all the same. In general, these contributions can be different. For example, in the case of the (112) peak, which has a multiplicity of 24, the contribution of the (112) peak is different from the contributions of the (211) and (121) peaks.

Figure S7 gives the intensity of the peaks (011), (002) and (112), i.e. the peaks with the lowest magnitudes of q, as a function of the azimuthal angle at $f_{12} = 1$ (the ratio used in the above presented calculation) and $f_{12} = 0.7$. It can be seen that the polarization dependence of the (112) peak depends on the value of f_{12}. If $f_{12} < 0.8$, the (112) peak has the same azimuthal intensity dependence as the peaks (011) and (002), which is in agreement with the experimental observations (see Fig. 3 in main text). The integrated intensity ($I^{(int)}$) of the (002) peak is higher than for the (011) peak, but they are still of the same order of magnitude: at $f_{12} = 1$, the ratio is

$I_{002}^{(int)}/I_{011}^{(int)} = 1.4$, at $f_{12} = 0.7$, the ratio is $I_{002}^{(int)}/I_{011}^{(int)} = 1.6$. Experimentally, the integrated intensity of the (011) peak is higher than $I^{(int)}$ of the (002) peak, but still of the same order of magnitude. Because of the crudeness of the model one can expect only qualitative agreement, so we do not find this discrepancy disturbing. The integrated intensity of the (112) peak is the lowest, which agrees with experimental observations.

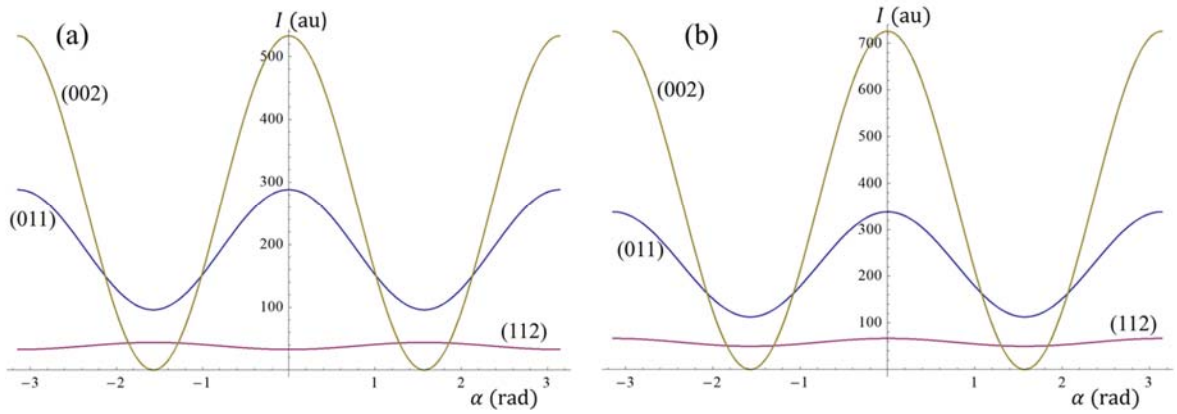

Fig. S7. The intensity (I) in arbitrary units (au) as a function of the azimuthal angle for the peaks (011), (002) and (112), which are the peaks with the lowest magnitudes of q; (a) $f_{12} = 1$, (b) $f_{12} = 0.7$.

2. *Materials and methods*

Materials:

All the studied compounds are dimers with an odd number of atoms in the linkage between the mesogenic cores, which induces a bent molecular geometry. Two of them, **AZO7** and **SB3**, are built from asymmetric molecules bearing a chiral, cholesteric unit, the third one, **CB7CB**, is a symmetric dimer (Fig. S8). The materials were synthesised at the University of Warsaw, the synthesis, purification and characterization was described previously [8].

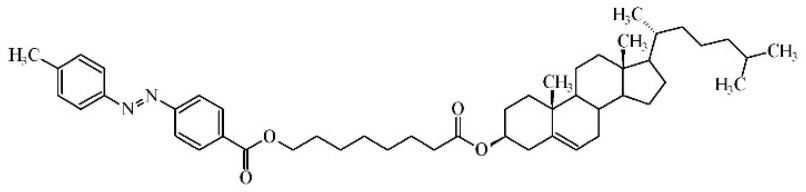

AZO7 Cr 64.0 N_{TB} 73.9 N^* 111.5 Iso

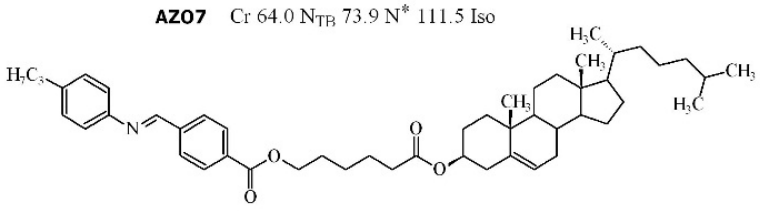

SB3 Cr 77.5 [N_{TB} 62.1] N^* 98.9 Iso

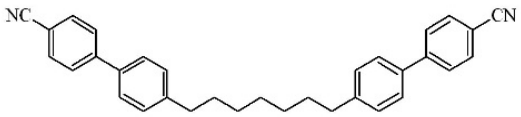

CB7CB Cr 76.4 N_{TB} 101.6 N 114.9 Iso

Fig. S8. Molecular structure of the studied compounds, **AZO7**, **SB3** and **CB7CB**. For each compound a phase sequence and phase transition temperatures determined by the differential scanning calorimetry (DSC) are given. Note, that for **AZO7** a narrow range of a blue phase between the N***** and Iso has been found by microscopic observations; however, it was not recorded on the DSC curves due to a limited resolution. Upon cooling the **AZO7** samples, the blue phase was metastable down to the transition to the NTB phase and thus the cholesteric phase was not observed.

Methods:

The x-ray experiments were performed on the soft x-ray scattering beam line (11.0.1.2) at the Advanced Light Source of Lawrence Berkeley National Laboratory. The x-ray beam was tuned to the K-edge of carbon absorption, ~280 eV (Fig. S9).

The x-ray beam with a cross-section of 300 × 200 μm was linearly polarized, with the polarization direction that can be continuously changed from the horizontal to vertical. Samples

with thickness lower than $1\,\mu$m were placed between two 100-nm-thick Si_3N_4 slides. The scattering intensity was recorded using the Princeton PI-MTE CCD detector, cooled to $-45°C$, having a pixel size of $27\,\mu$m, with an adjustable distance from the sample. The detector was translated off axis to enable a recording of the diffracted x-ray intensity. The adjustable position of the detector allowed to cover a broad range of q vectors, corresponding to periodicities from approximately $5.0 - 300$ nm.

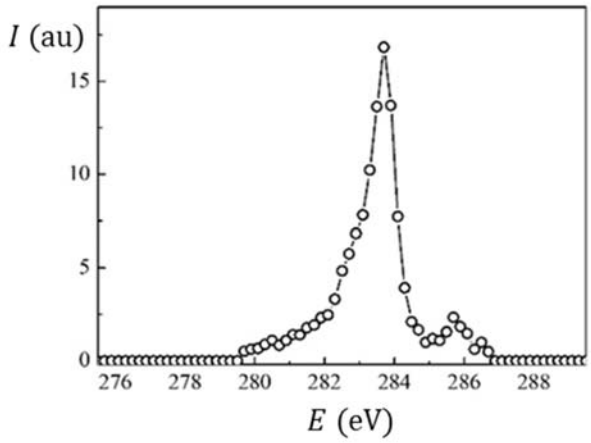

Fig. S9. Intensity (I) of the signal in the N_{TB} phase as a function of the energy (E) of the x-ray beam, measured for AZO7 compound.

The AFM images were taken with the Bruker Dimension Icon microscope, working in the tapping mode at the liquid crystalline-air surface. Cantilevers with a low spring constant, $k = 0.4$ N/m were used, the resonant frequency was in a range of $70 - 80$ kHz, a typical scan frequency was 1 Hz. Samples for the AFM imaging were prepared in glass cells at elevated temperature, quenched to room temperature and unsealed.

3. *Additional experimental results*

In both, the N_{TB} and N* phase of chiral dimer **SB3** the resonant diffraction signal shows only a weak temperature dependence (Fig. S10).

For the achiral dimer **CB7CB** the heliconical structure changes critically when temperature approaches the transition to the non-modulated nematic phase, while in the crystalline phase the resonant signal related to the helical structure was found to be temperature independent (Fig. S11). For the **AZO7** material a direct transition from the BPI to N_{TB} phase was observed on cooling, with a small temperature range in which both phases coexists (Fig. S12).

The AFM image of **SB3** recorded at the ambient temperature shows that an additional structure with a longer periodicity ($50 - 80$ nm) is present in the N_{TB} phase (Fig. S13).

The AFM images taken at a room temperature of the crystalline and metastable N_{TB} phase of **CB7CB** are shown in Fig. S14. Both phases are characterized by ~8 nm periodicities, however in the case of a crystalline phase no focal conics were found. The fast Fourier transform (FFT) obtained from the image registered in the crystalline phase shows the first and second harmonic, and both are of almost equally intensity. On the other hand, the FFT obtained from the image registered in the N_{TB} phase shows only the first harmonic.

The position of the RSoXS signal in the N_{TB} phase of the **AZO7** compound is temperature dependent (Fig. S15).

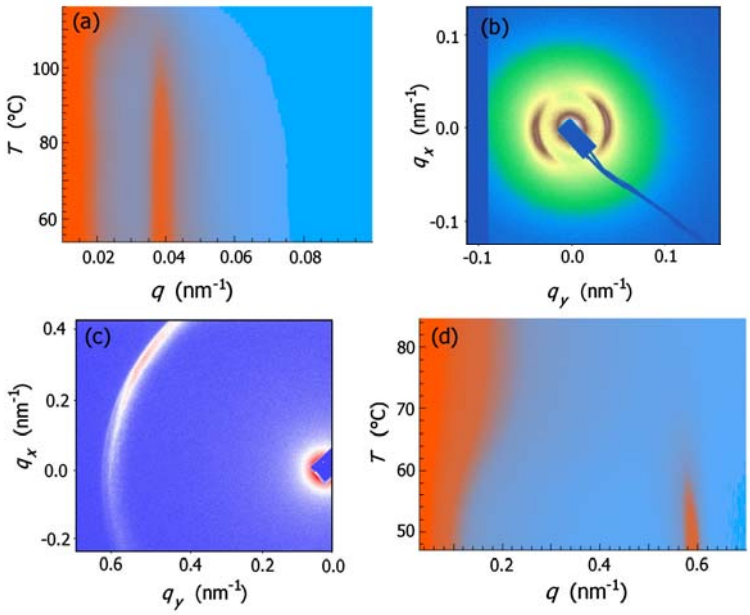

Fig. S10. Temperature dependence of the RSoXS pattern measured for **SB3** compound in the temperature range of the (a) N* and (d) N_{TB} phase. The patterns were obtained in the consecutive cooling/heating runs with modified experimental conditions (different detector position). (b) and (c) give the 2D RSoXS patterns taken in the N* and N_{TB} phase, respectively.

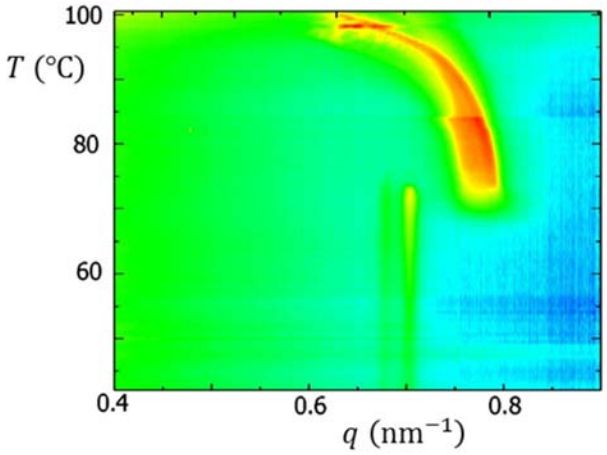

Fig. S11. Temperature evolution of the RSoXS signal for the **CB7CB** sample, measured on heating. Note that while in the crystalline phase the signal position is practically temperature independent, in the N_{TB} phase it changes strongly due to the changes of the heliconical pitch, from 8 to 10 nm upon approaching the transition to the N phase.

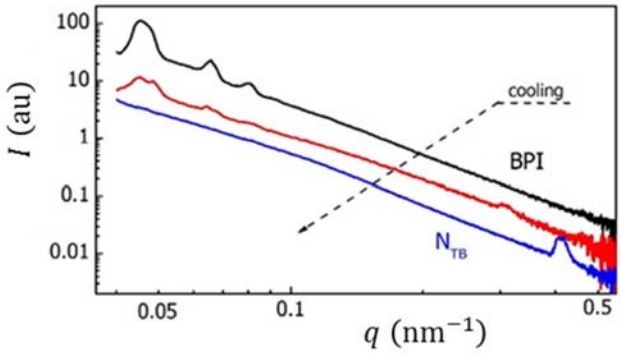

Fig. S12. RSoXS patterns, scattered intensity (I) in arbitrary units (au) as a function of the magnitude of the scattering vector q, for the **AZO7** compound recorded in a broad q range. On cooling, a direct transition from the BPI (black line) to the N_{TB} phase (blue line) is observed with a small (1 K) temperature range of the phase coexistence (red line).

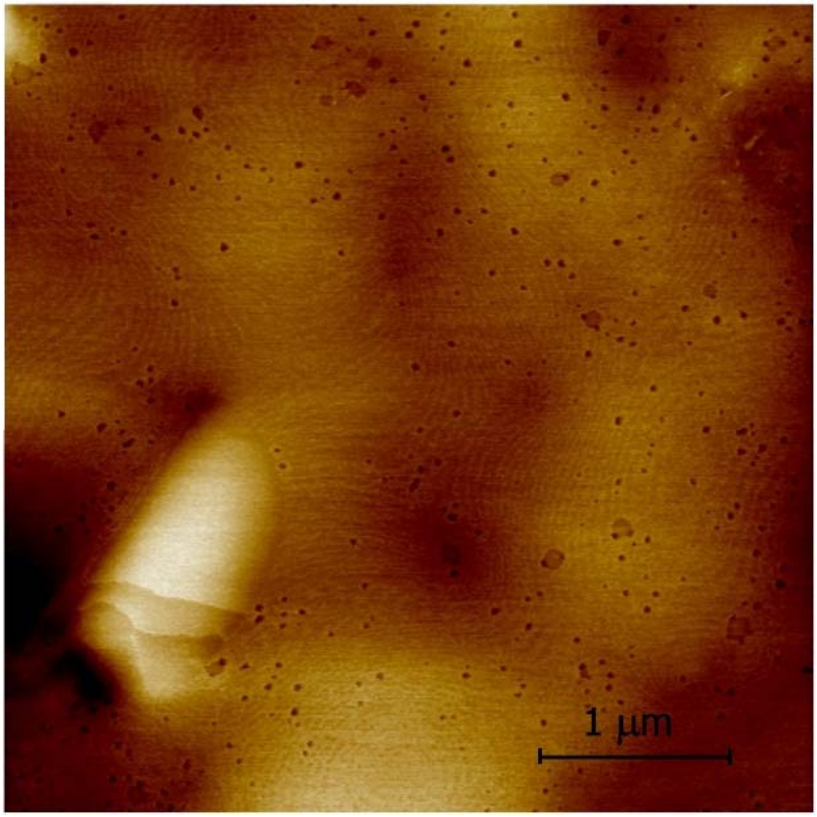

Fig. S13. AFM image taken in the N_{TB} phase of **SB3** compound at room temperature. The distance between the lines is approximately 50-80 nm.

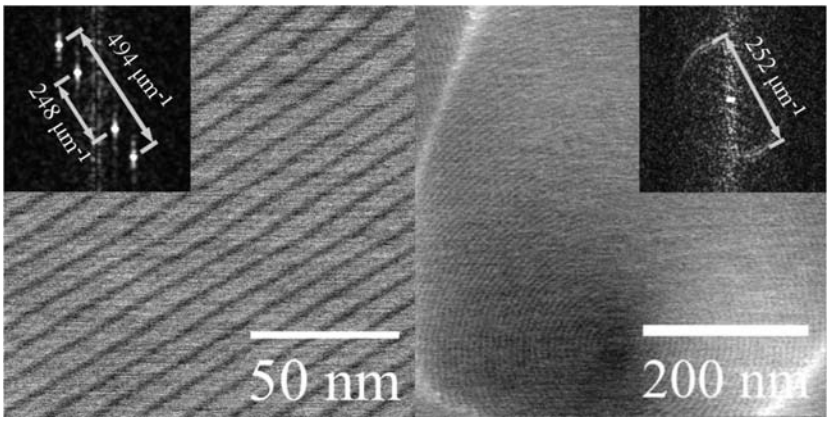

Fig. S14. AFM images of **CB7CB** in a crystal (left) and N_{TB} (right) phase and the corresponding fast Fourier transform patterns. In the crystalline phase the intensity of the first and second harmonic of the detected periodicity (8.06 nm) is of the same order of magnitude. In the N_{TB} phase only a weak first harmonic (7.93 nm) is detected.

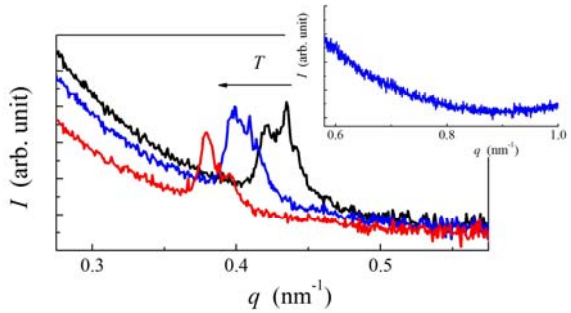

Fig. S15: RSoXS patterns, the intensity (*I*) in arbitrary units as a function of the magnitude of the scattering vector *q*, for the **AZO7** compound in the N_{TB} phase at three different temperatures. The inset: the *q*-range at which the 2*q*0 signal is expected (recorded with a different detector position).

REFERENCES

[1] D. H. Templeton and L. K. Templeton, *Acta Crystallogr. Sect. A* **36**, 237 (1980).

[2] V. E. Dmitrienko, *Acta Crystallogr. Sect. A* **39**, 29 (1983).

[3] A. M. Levelut and B. Pansu, *Phys. Rev. E* **60**, 6803 (1999).

[4] C. Meyer, G. R. Luckhurst, and I. Dozov, *J. Mater. Chem. C* **3**, 318 (2015).

[5] D. H. Templeton and L. K. Templeton, *Acta Crystallogr. Sect. A* **38**, 62 (1982).

[6] V. E. Dmitrienko, *Acta Crystallogr. Sect. A* **40**, 89 (1984).

[7] H. Yoshida, https://www.youtube.com/watch?v=NJG14FdcWkg

[8] E. Gorecka, N. Vaupotič, A. Zep, D. Pociecha, J. Yoshioka, J. Yamamoto and H. Takezoe, *Angew. Chem. Int. Ed.* **54**, 10155 (2015).